Tyrannosaurid Skeletal Design First Evolved at Small Body Size

Paul C. Sereno,[1]* Lin Tan,[2] Stephen L. Brusatte,[3] Henry J. Kriegstein,[4] Xijin Zhao,[5] Karen Cloward[6]

Nearly all of the large-bodied predators (>2.5 tons) on northern continents during the Late Cretaceous were tyrannosaurid dinosaurs. We show that their most conspicuous functional specializations—a proportionately large skull, incisiform premaxillary teeth, expanded jaw-closing musculature, diminutive forelimbs, and hindlimbs with cursorial proportions—were present in a new, small-bodied, basal tyrannosauroid from Lower Cretaceous rocks in northeastern China. These specializations, which were later scaled up in Late Cretaceous tyrannosaurids with body masses approaching 100 times greater, drove the most dominant radiation of macropredators of the Mesozoic.

Tyrannosaurus rex is the best-known of several tyrannosaurid species (*1*), which were dominant in their role as multi-ton predators on northern continents during the final 25 million years of the Mesozoic (*2*–*4*). Hallmark tyrannosaurid adaptations include a relatively large skull with enhanced jaw-closing musculature, enlarged olfactory bulbs, a relatively miniaturized forelimb with only two functional digits, and a pinched pedal structure common to cursors—features presumed to have evolved for hypercarnivory (strict carnivory) at large body size. Tyrannosaurids have been viewed as heterochronic "peramorphs" (*5*), the largest of which grew beyond the size and form of smaller-bodied ancestors (*6*) via developmental acceleration (*7*).

In the past decade, fossils pertaining to earlier and more primitive tyrannosauroid species have been discovered in rocks of Middle Jurassic to Early Cretaceous age in North America, Europe, and China, including *Guanlong* (*8*), *Dilong* (*5*), and *Xiongguanlong* (*9*) and the more fragmentary *Eotyrannus* (*10*), *Stokesosaurus* (*11*), *Aviatyrannis* (*12*), and *Proceratosaurus* (*13*). With body lengths of only 2 to 5 m, these finds confirmed that tyrannosaurids evolved from small-bodied, long-armed "tyrannoraptors" (*1*, *4*, *10*). Evidence linking these precursors to their oversized descendants has been limited to a relatively small set of derived features in the skull and skeleton (*5*, *8*, *9*). On the other hand, it has been thought that the much greater range of truly tyrannosaurian characters, particularly those in the skull and limbs, evolved only with body size increase in Late Cretaceous tyrannosaurids (*14*).

We describe here a new small-bodied theropod, *Raptorex kriegsteini* nov. gen. nov.

[1]Department of Organismal Biology and Anatomy, University of Chicago, Chicago, IL 60637, USA. [2]Long Hao Institute of Geology and Paleontology, Bureau of Land and Resources, 010010 Hohhot, People's Republic of China (PRC). [3]Division of Paleontology, American Museum of Natural History, New York, NY 10024, USA. [4]3 Evergreeen Lane, Higham, MA 02043, USA. [5]Institute of Vertebrate Paleontology and Paleoanthropology, Chinese Academy of Sciences, 100044 Beijing, PRC. [6]Western Paleontological Laboratories, Lehi, UT 84043, USA.

*To whom correspondence should be addressed. E-mail: dinosaur@uchicago.edu

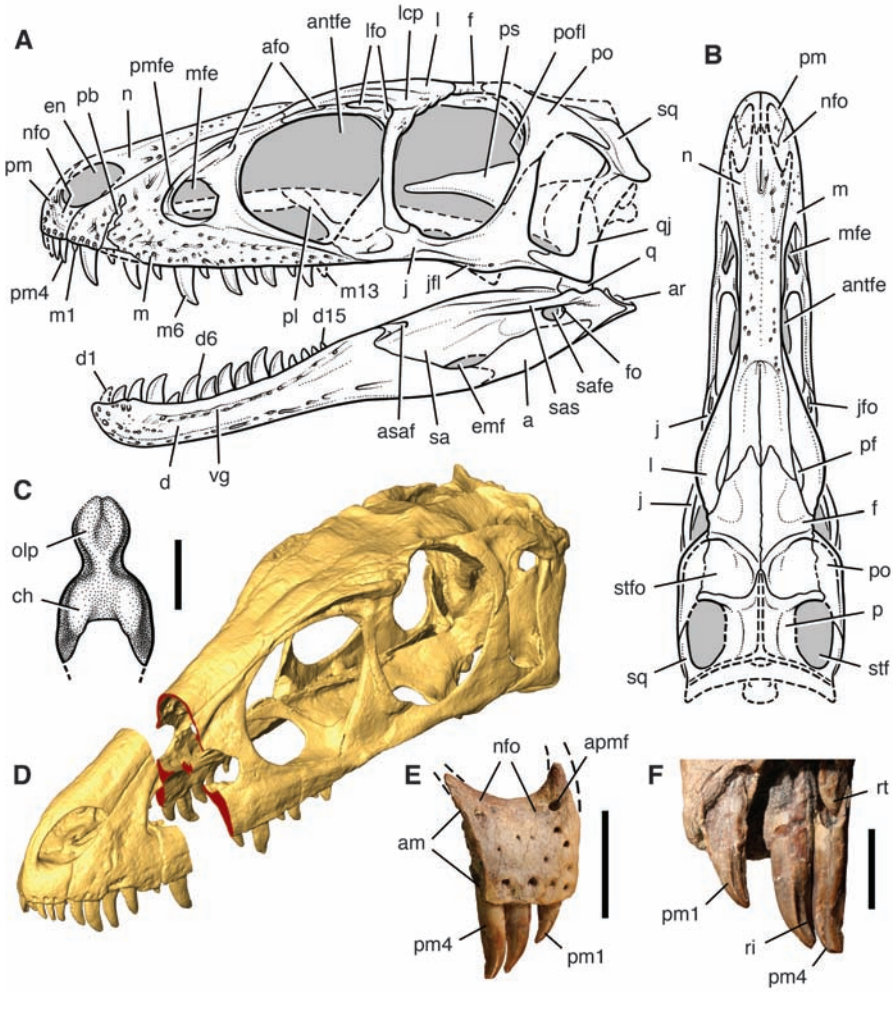

Fig. 1. Skull, endocast, and premaxillary teeth of the Early Cretaceous tyrannosauroid *R. kriegsteini*. The skull reconstruction in (**A**) lateral and (**B**) dorsal views is shown. (**C**) Partial endocast in dorsal view showing the enlarged olfactory peduncles and swollen cerebral hemispheres. (**D**) Skull model composed of cast bones as seen in a computed tomography scan showing a cross section (red) of the snout at mid-length. (**E**) Right premaxilla in lateral view. (**F**) Right premaxillary crowns in posteromedial view. Abbreviations: a, angular; afo, accessory fossa; am, articular surface for the maxilla; antfe, antorbital fenestra; apmf, anterior premaxillary foramen; ar, articular; asaf, anterior surangular foramen; ch, cerebral hemisphere; d, dentary; d1, d6, and d15, dentary tooth 1, 6, and 15; emf, external mandibular fenestra; en, external naris; f, frontal; fo, foramen; j, jugal; jfl, jugal flange; jfo, jugal fossa; lcp, lacrimal cornual process; l, lacrimal; lfo, lacrimal fossa; m, maxilla; m1, m6, and m13, maxillary tooth 1, 6, and 13; mfe, maxillary fenestra; n, nasal; nfo, narial fossa; olp, olfactory peduncle; p, parietal; pb, pathologic bone; pf, prefrontal; pl, palatine; pm, premaxilla; pm1 and pm4, premaxillary tooth 1 and 4; pmfe, promaxillary fenestra; po, postorbital; pofl, postorbital flange; ps, parasphenoid; q, quadrate; qj, quadratojugal; ri, ridge; rt, replacement tooth; sa, surangular; safe, surangular fenestra; sas, surangular shelf; sq, squamosal; stf, supratemporal fenestra; stfo, supratemporal fossa; vg, vascular groove. Scale bars, 3 cm in (C), 2 cm in (E), and 1 cm in (F).

sp. (*15*), that exhibits all major tyrannosaurid functional specializations in the skull and skeleton (Figs. 1 and 2), including a diminutive forelimb (Fig. 3). Discovered in the Lujiatun Beds [Hauterivian-Barremian stages, ~130 million years ago (Ma)] of the Lower Cretaceous Jehol Group in northeast China (*15*, *16*), *Raptorex* is known from an articulated skeleton of a subadult or young adult approximately 5 to 6 years old, with an adult body length of no more than 3 m (*16*).

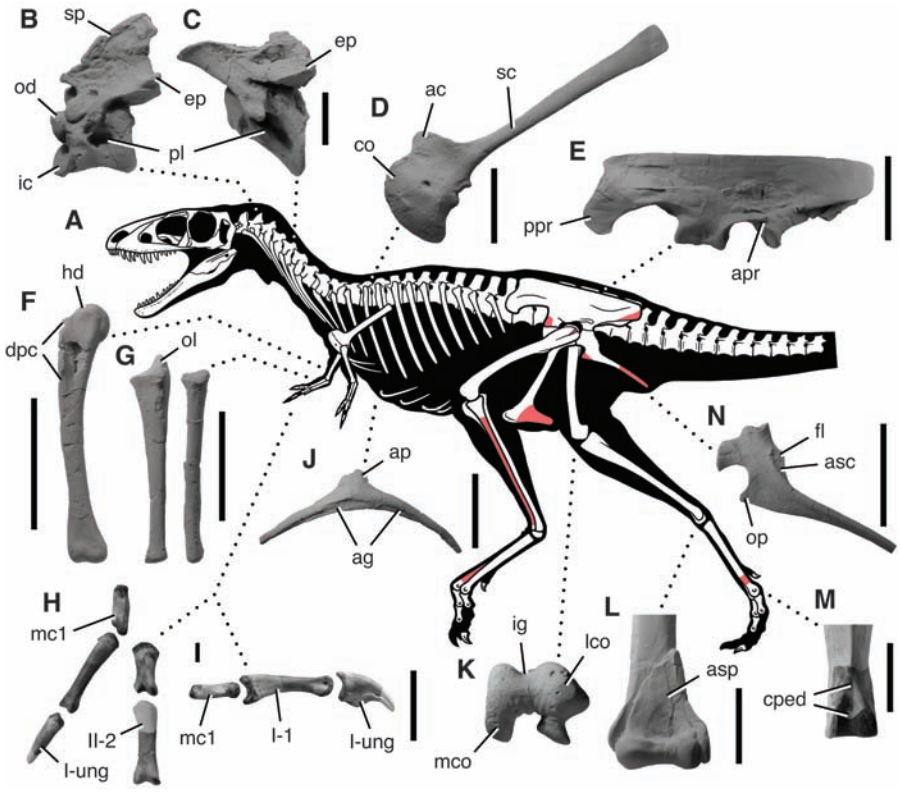

Fig. 2. Postcranial features of the Early Cretaceous tyrannosauroid *R. kriegsteini*. (**A**) Skeletal silhouette showing preserved bones (missing portions shown in red; the cast of the bones was used to eliminate color distractions). (**B**) Axis (C2) in left lateral view. (**C**) Midcervical vertebra (C5) in left lateral view. (**D**) Scapulocoracoid (left) in lateral view. (**E**) Ilium (left) in lateral view. (**F**) Humerus (left) in anterior view. (**G**) Ulna and radius (left) in medial view. (**H**) Manus (right) in dorsal view. (**I**) Manual digit I (right) in medial view. (**J**) Co-ossified anterior gastral elements in ventral view. (**K**) Femur (left) in distal view. (**L**) Distal tibia and astragalus (left) in anterior view. (**M**) Distal metatarsal 3 (right) in posterior view. (**N**) Proximal ischium (left) in lateral view. Abbreviations: I-1, manual digit I phalanx 1; I-ung, manual digit I ungual; II-2, manual digit II phalanx 2; ac, acromion; ag, articular surface for successive gastralium; ap, anterior process; apr, acetabular process; asc, attachment scar; asp, ascending process; co, coracoid; cped, condylar pedicel; dpc, deltopectoral crest; ep, epipophysis; fl, flange; hd, head; ic, intercentrum; ig, intercondylar groove; mc1, metacarpal 1; mco, medial condyle; lco, lateral condyle; od, odontoid; ol, olecranon; op, obturator process; pl, pleurocoel; ppr, pendant process; sc, scapula; sp, spine. Scale bars, 2 cm in (B), (C), (H), and (I); 3 cm in (M); 5 cm in (D), (F), (G), and (J) to (L); 10 cm in (E) and (N).

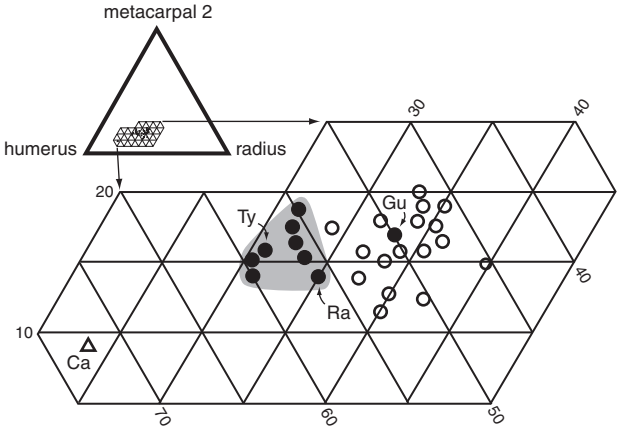

Fig. 3. Ternary morphospace plot for principal forelimb segments (humerus, radius, and metacarpal 2) as percentages of total forelimb length in nonavian theropods, showing *Raptorex* near *Tyrannosaurus* and other short-armed tyrannosaurids (gray tone) and *Guanlong* among nontyrannosaurid theropods with relatively unreduced forelimbs. Open circles are nontyrannosaurid theropods; solid dots are tyrannosauroids; the open triangle is the abelisaurid *Carnotaurus*. The three nontyrannosaurid theropods (open circles) closest to the tyrannosauroid cluster are coelophysoids (*Coelophysis* and *Syntarsus*). Data are from (*2*, *8*, *27*). Abbreviations: Ca, *Carnotaurus*; Gu, *Guanlong*; Ra, *Raptorex*; Ty, *Tyrannosaurus*.

Many features place *Raptorex* within Tyrannosauroidea, a clade including Tyrannosauridae and their closest relatives (Fig. 4). In the skull, for example, the premaxilla is anteroposteriorly short and bears teeth with incisiform crowns, the maxilla has only 13 teeth, the internasal suture is fused, the jugal has a marked inflection along its ventral margin, and the retroarticular process of the lower jaw is short and transversely broad (Fig. 1, A and B, and D to F). In the postcranial skeleton, likewise, the scapula has a strap-shaped blade, and the forelimb and ilium are relatively short and long, respectively. The principal phylogenetic question, rather, is where *Raptorex* falls within Tyrannosauroidea.

The skull is proportionately large as in tyrannosaurids, measuring approximately 40% of trunk length (Fig. 2A). The skull in most other theropods, including the basal tyrannosauroid *Guanlong* (*8*), is relatively smaller, measuring about 30% or less of trunk length (*16*). Many additional cranial characters link *Raptorex* and large-bodied tyrannosaurids. The functional significance of some of these characters is poorly understood, such as the textured, highly vascularized nasals (also in *Eotyrannus*), the sutural contact between the lacrimal and frontal along the orbital margin, the pneumatic invasion of the bodies of the lacrimal and squamosal, or the enlarged surangular foramen (Fig. 1, A and B) (*16*).

Strengthening of the skull roof, on the other hand, is clearly the functional role of another suite of advanced cranial characters linking *Raptorex* and large-bodied tyrannosaurids (*17*, *18*). The nasals are more strongly transversely arched (Fig. 1D) than in the basal tyrannosauroids *Dilong* (*5*) or *Xiongguanlong* (*9*), and the sutural surface between the nasal and maxilla is corrugated as in tyrannosaurids (*3*, *19*) rather than planar. The antorbital fenestra, in addition, is proportionately short and lacks any nasal contribution to its dorsal margin, as in tyrannosaurids (*3*, *19*, *20*).

The functional role of another suite of advanced cranial characters linking *Raptorex* and large-bodied tyrannosaurids involves the expansion of attachment sites for jaw-closing (adductor) musculature. The supratemporal fossae in *Raptorex* extend broadly onto the frontals and meet along a median sagittal crest, which is particularly prominent anteriorly (Fig. 1, B and D). Attachment site expansion for adductor musculature also includes a flange on the dorsal aspect of the squamosal and a prominent surangular shelf at the posterior end of the lower jaw (Fig. 1A).

Differentiation of a set of smaller, incisiform teeth at the anterior end of the upper jaw is another functional specialization shared by *Raptorex* and tyrannosaurids. The last premaxillary tooth

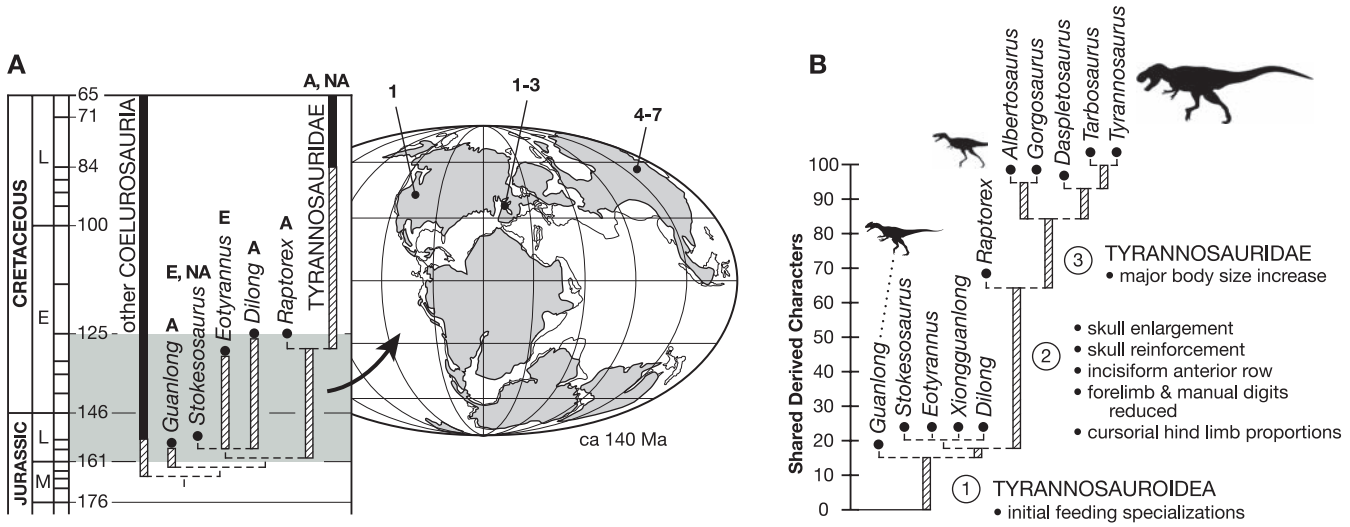

Fig. 4. Temporal, geographic, and phylogenetic patterns among tyrannosauroids. (**A**) Temporally calibrated phylogeny of tyrannosauroids based on phylogenetic analysis (*16*), showing an early diversity of basal tyrannosauroids (shaded) from localities across Laurasia and plotted on an Early Cretaceous paleogeographic map (*28*). *Proceratosaurus* (*13*) and *Xiongguanlong* (*9*) were excluded from this plot because of limited available morphologic data and age uncertainty, respectively. (**B**) Phylogram scaled to the amount of character change (delayed transformation) based on cladistic analysis of 101 characters in 11 tyrannosauroids (consensus of 28 minimum-length trees of 123 steps; consistency index = 0.862, retention index = 0.954) (*16*). Circled nodes 1 to 3 outline major transformations in tyrannosauroid evolution. Taxonomic definitions (*1*) of Tyrannosauroidea, Tyrannosauridae, and other taxa follow (*29*). Abbreviations for biogeographic area and localities: A, Asia; E, Europe; NA, North America; 1, *Stokesosaurus*; 2, *Proceratosaurus* and *Eotyrannus*; 3, *Aviatyrannis*; 4, *Guanlong*; 5, *Dilong*; 6, *Xiongguanlong*; 7, *Raptorex*.

is substantially smaller than the first maxillary tooth, and all four premaxillary crowns are incisiform (with a D-shaped cross section) with a posteriorly facing median ridge (Fig. 1, A, E, and F). In the basal tyrannosauroids *Guanlong* (*8*) and *Dilong* (*5*), in contrast, tooth size is gradational to the maxillary series, and only the anterior two premaxillary teeth have a D-shaped cross section and a discrete posterior ridge (*16*). The maxillary crowns in *Raptorex*, nevertheless, remain transversely compressed as in other basal tyrannosauroids, unlike the stout, subcylindrical crowns in mature tyrannosaurids (*20*).

A partial endocast shows enlarged, semicircular olfactory bulbs with a volume of approximately 2.5 cm^3 situated adjacent to one another in the midline (Fig. 1C). The olfactory bulbs are 60% of the maximum width of the cerebral hemispheres and nearly 20% of their volume, which is significantly larger than in other nonavian coelurosaurs (*21*, *22*) but resembles the enlarged condition in tyrannosaurids (*23*). The swollen cerebral hemispheres each have a volume of approximately 14.0 cm^3, which is approximately 60% of the hemispherical volume in *Allosaurus* (*24*), a theropod with a body mass (~1000 kg) at least 10 times that of *Raptorex* (~60 to 100 kg, comparable to *Deinonychus*) (*24*, *25*). Thus, it appears that the cerebrum in *Raptorex*, as in tyrannosaurids and other nonavian coelurosaurs, is relatively large. *Raptorex*, however, lacks the long olfactory stalk and undivided cerebrum of tyrannosaurids, which are best interpreted as size-related features arising independently in large-bodied theropods (*22*).

The vertebral column can be partitioned into 10 cervical, 13 dorsal, and 5 co-ossified sacral vertebrae, as well as the first 11 caudal vertebrae of the tail (Fig. 2A) (*16*). The vertebral column is not a skeletal division that exhibits marked modification in tyrannosauroids, and *Raptorex* and other basal tyrannosauroids show few modifications particular to tyrannosaurids. The cervical centra are opisthocoelous and have relatively longer centra and lower spinous processes than in tyrannosaurids (Fig. 2, B and C). A pneumatopore (pleurocoel) is present on the sides of all presacral centra and most of the sacrals, as in tyrannosaurids and in contrast to the more limited axial pneumaticity in *Guanlong* (*8*). The gastral cuirass (stomach ribs), in contrast to the vertebrae, show modifications found only in tyrannosaurids. The anteriormost segment, which is composed of fused medial elements, has a subtriangular anteromedian process and a posterior articular groove for contact with the next pair of gastral elements (Fig. 2J) (*2*).

The scapulocoracoid has a prominent acromial process and narrow, strap-shaped blade, closely resembling the condition in tyrannosaurids as compared to the basal tyrannosauroids *Guanlong* and *Dilong* (Fig. 2D). The diminutive forelimb, likewise, is remarkably similar to that in tyrannosaurids and unlike the longer forelimb of *Guanlong*, which resembles that in other basal coelurosaurs such as *Ornitholestes*. The humerus has a subspherical head and reduced deltopectoral crest, and the ulna has a prominent olecranon process, straight shaft, and flat distal end (Fig. 2, F and G). The partially preserved manus also shows advanced features shared with tyrannosaurids, in contrast to that in *Guanlong* and *Dilong*, such as the reduction of metacarpal 1 (length subequal to the first phalanx of the digit II, medial distal condyle rudimentary) and lengthening of the first phalanx of digit I (Fig. 2H). The small size of the first metacarpal and the very close correspondence in form of this metacarpal and the preserved manual phalanges to those in tyrannosaurids (*2*) suggest that the manus was probably functionally didactyl.

The relative length and proportions within the forelimb of *Raptorex* correspond well with those in tyrannosaurids. Humeral length is 29% that of the femur in *Raptorex* and tyrannosaurids, which is substantially shorter than in the basal tyrannosauroids *Guanlong* (63%) and *Dilong* (53%) (Table 1). Within the forelimb, the humerus is longer relative to either the radius or metacarpus, constituting nearly 60% of forelimb length rather than 50% as in *Guanlong*. Proportional variation within the forelimb is best visualized on a ternary plot summarizing the percentage contribution to forelimb length of the humerus, radius, and metacarpal 2 (Fig. 3). *Raptorex* plots near a cluster of tyrannosaurids with distinctive forelimb proportions, whereas *Guanlong* plots in the middle of an array of nontyrannosaurid, nonavian theropods.

The pelvic girdle of *Raptorex* exhibits derived features shared with tyrannosaurids that are absent in other basal tyrannosauroids such as *Guanlong* (*8*), *Stokesosaurus* (*11*), *Dilong* (*5*), and *Xiongguanlong* (*9*). The elongate ilium has a straight dorsal margin that appears to be pressed against the sacral neural spines, and a marked antitrochanter is present on the supraacetabular shelf, which does not project laterally beyond the ischial peduncle (Fig. 2E). The ischium exhibits a prominent rugose flange for muscle attachment and a narrow tapering shaft (Fig. 2N), and the

Table 1. Skull and long-bone lengths (in centimeters, upper portion) and proportions (in %, lower portion) of *R. kriegsteini* and other tyrannosauroids (*2*, *5*, *8*, *30*). Parentheses indicate estimates; dashes indicate missing data. Measurements average long-bone lengths when both sides are available.

Measure or ratio	*Guanlong* IVPP V14531	*Dilong* IVPP V14243	*Raptorex* LH PV18	*Albertosaurus* AMNH 5664	*Tyrannosaurus* FM PR2081
Skull	36.3	16.6	(30.0)	67.8	139.4
Humerus	26.3	9.6	9.9	20.5	38.5
Radius	17.8	—	5.2	10.0	17.3
Metacarpal 2	8.9	—	(2.4)‡	6.0	10.4
Femur	41.6	18.0	33.8	70.0	131.5
Tibia	42.4	19.9	39.7	74.8	114.3
Metatarsal 2	34.0	11.2	24.5	(41.8)§	58.4
Metatarsal 4	36.0	11.1	26.6	(44.6)§	62.1
Humerus/femur	63%	53%	29%	29%	29%
Humerus/forelimb*	50%	—	56%	56%	58%
Radius/forelimb	33%	—	30%	27%	26%
Metacarpal 2/forelimb	17%	—	14%	16%	16%
Tibia/femur	102%	111%	118%	107%	87%
Femur/hindlimb†	35%	37%	34%	37%	43%
Tibia/hindlimb	35%	40%	40%	40%	37%
Metatarsal 4/hindlimb	30%	23%	26%	23%	20%

*Forelimb length equals the sum of the humerus, radius, and metacarpal 2. †Hindlimb length equals the sum of the femur, tibia, and metatarsal 4. Metatarsal 4 is used because only the distal end of metatarsal 3 is preserved in *Raptorex*. ‡Estimated from metacarpal 1, based on the metacarpal ratio in *Tyrannosaurus* FM PR2081 (*2*). §Estimated from metatarsal 3, based on the metatarsal ratio in *Tyrannosaurus* FM PR2081 (*2*).

pubis has a distal foot with a prominent anterior ramus (Fig. 2A).

The hindlimb in *Raptorex* also exhibits several derived features and proportions shared with tyrannosaurids. The femoral anterior trochanter extends proximally as far as the greater trochanter, the femoral distal condyles are deeply divided fore and aft (Fig. 2K), and the ascending process of the astragalus is tall (Fig. 2L). Metatarsal 3 is wedge-shaped (arctometatarsalian) proximally and has a raised nonarticular platform adjacent to the condyles distally (Fig. 2M). Within the hindlimb, tibial length is 118% that of the femur, a longer proportion than has been recorded in any other tyrannosauroid (Table 1).

Phylogenetic analysis of Tyrannosauroidea (*16*) (Fig. 4) confirms the basal position of *Guanlong*, *Stokesosaurus*, *Eotyrannus*, *Dilong*, and *Xiongguanlong* relative to *Raptorex* and Tyrannosauridae (*5*, *8*–*10*). Although a few synapomorphies support *Guanlong* as the basalmost tyrannosauroid and *Xiongguanlong* as closer to *Raptorex* and Tyrannosauridae, relationships among these five basal tyrannosauroids remain poorly resolved and collapse with one additional step (Fig. 4B). Many derived features, in contrast, provide strong support for positioning *Raptorex* as the sister taxon to a monophyletic Tyrannosauridae. With only a few autapomorphies evident in its skeletal anatomy (*15*), *Raptorex* closely approximates a hypothetical ancestor on the lineage leading to Tyrannosauridae.

Three major morphological stages can now be visualized in the evolutionary history of Tyrannosauroidea (Fig. 4B). The first stage includes tyrannosauroids of Middle Jurassic to Early Cretaceous age with a trans-Laurasian distribution that are of small to medium body size and exhibit some initial feeding specializations. They include the Middle Jurassic genus *Proceratosaurus* (*13*); the Late Jurassic genera *Guanlong* (*8*), *Stokesosaurus* (*11*), and *Aviatyrannis* (*12*); and the Early Cretaceous genera *Eotyrannus* (*10*), *Dilong* (*5*), and *Xiongguanlong* (*9*) (Fig. 4A, shading). Femoral length, a rough proxy for body size, varies from 18 cm in *Dilong* (*5*) to 67 cm in *Stokesosaurus* (*11*) and is always less than that among subadult or adult tyrannosaurids (approximately 70 to 130 cm) (Table 1). Diagnostic tyrannosauroid features in this first stage involve initial strengthening of the snout via internasal fusion, specialization of the anteriormost upper teeth as incisors, and initial enlargement of the attachment area for jaw-closing musculature. In most other respects, the functional specializations seen in tyrannosaurids are lacking in the most complete of these early tyrannosauroids (*5*, *8*, *10*, *11*).

The second stage involves the most conspicuous functional specializations of tyrannosaurids: a proportionately large skull with accessory pneumatization, a set of incisiform premaxillary teeth more distinctive in size and form, expanded jaw-closing musculature operating jaws with fewer teeth, a diminutive forelimb with distinctive intralimb proportions and joint morphology, and an elongate hindlimb with cursorial proportions and a fully developed compact-splint (arctometatarsalian) metatarsus (Fig. 4, node 2). All are manifest in *Raptorex*, a possible contemporary of the more primitive tyrannosauroid *Dilong*, from Lower Cretaceous rocks dating to about 125 Ma—some 40 million years before the oldest known tyrannosaurid (Fig. 4A).

The third stage, comprising currently known tyrannosaurids, is characterized by a marked increase in body size (Fig. 4, node 3). Some features, such as the more robust cheek teeth with subcylindrical cross section, distinguish tyrannosaurids from other large theropods such as spinosaurids and carcharodontosaurids. Many of the now more limited set of derived features that characterize tyrannosaurids, however, may owe their appearance to size increase, such as bony flanges within the orbit and laterotemporal openings, the prominence of occipital and vertebral processes for attachment to cervical musculature, the relative shortening of vertebral length, and less cursorial limb proportions. Adult body length in *Raptorex* is 3 m or less, corresponding to a body mass of approximately 65 kg, based on estimates for similar-sized theropods such as *Velociraptor*, *Deinonychus*, and *Oviraptor* (*16*, *25*, *26*). Tyrannosaurids, in contrast, range in body length from 6 to 12 m, corresponding to a body mass range of 2500 to 6000 kg (*16*, *25*, *26*). Body mass thus increased at least 40-fold from that in *Raptorex* to basal tyrannosaurids and eventually more than 90-fold to that in *Tyrannosaurus*.

Raptorex, in sum, reveals that the tyrannosaurid morphotype—the oversized skull, muscle-bound jaws, tiny forelimbs, and fleet-footed hindlimbs—evolved at modest body size some 125 million years ago (Fig. 4A). These features, singly or in concert, can no longer be explained as a passive allometric consequence of body size increase or the product of an extended (peramorphic) growth trajectory (*5*, *14*). Instead, these features seem first to have evolved as an efficient predatory strategy at relatively small body size. It remains to be seen whether miniature precursors such as *Raptorex* eventually will be discovered for other large-bodied predatory radiations among dinosaurs, such as abelisaurids, spinosauroids (megalosauroids), and carcharodontosaurids. For tyrannosauroids, the predatory skeletal design embodied in *Raptorex* was scaled up with little modification in descendants with body mass as much as 90 times greater.

References and Notes

1. We use the following phylogenetic definitions: **Tyrannoraptora**, the least inclusive clade containing *Tyrannosaurus rex* Osborn 1905 and *Passer domesticus* (Linnaeus 1758); **Tyrannosauroidea**, the most inclusive clade containing *Tyrannosaurus rex* Osborn 1905 but not *Ornithomimus edmontonicus* Sternberg 1933, *Troodon formosus* Leidy 1856, *Velociraptor mongoliensis* Osborn 1924; **Tyrannosauridae**, the least inclusive clade containing *Tyrannosaurus rex* Osborn 1905 and *Gorgosaurus libratus* Lambe 1914, *Albertosaurus sarcophagus* Osborn 1905.
2. C. A. Brochu, *J. Vert. Paleontol. Mem. 7* **22**, 1 (2002).
3. P. J. Currie, *Acta Palaeontol. Pol.* **48**, 191 (2003).
4. T. R. Holtz Jr., in *The Dinosauria*, D. B. Weishampel, P. Dodson, H. Osmólska, Eds. (Univ. of California Press, Berkeley, CA, 2004), pp. 111–136.
5. X. Xu *et al.*, *Nature* **431**, 680 (2004).
6. T. R. Holtz Jr., *J. Paleontol.* **68**, 1100 (1994).
7. G. M. Erickson *et al.*, *Nature* **430**, 772 (2004).
8. X. Xu *et al.*, *Nature* **439**, 715 (2006).
9. D. Li, M. A. Norell, K. Q. Gao, N. D. Smith, P. J. Makovicky, *Proc. R. Soc. London Ser. B* 10.1098/rspb.2009.0249 (2009).

10. S. Hutt, D. Naish, D. M. Martill, M. J. Barker, P. Newbery, *Cretac. Res.* **22**, 227 (2001).
11. R. B. J. Benson, *J. Vert. Paleontol.* **28**, 732 (2008).
12. O. W. M. Rauhut, *Palaeontol.* **46**, 903 (2003).
13. O. W. M. Rauhut, A. Milner, *J. Vert. Paleontol.* **28**, 130A (2008).
14. E. Stokstad, *Science* **306**, 211 (2004).
15. **Etymology**: *raptor*, plunderer (Greek); *rex*, king (Greek); *kriegsteini*, after Roman Kriegstein, in whose honor the specimen was secured for scientific study. **Holotype**: LH PV18, partially articulated skeleton composed of disarticulated cranial bones representing most of the skull and postcranial skeleton, lacking portions of the forelimb and the distal one-half of the tail (beyond the 11th caudal). The holotype represents a young adult, as shown by fusion of the nasals and braincase elements in the skull and at least partial fusion of all neurocentral sutures. Cataloged in the collection of the Long Hao Institute of Geology and Paleontology (Hohhot, Nei Mongol Autonomous Region) and the University of Chicago (Chicago). **Locality**: Approximately 41°20′N and 119°40′E, collected privately in the border area between Liaoning Province and the Nei Mongol Autonomous Region of the People's Republic of China. **Horizon and associations**: Lujiatun Beds of the Yixian Formation, comprising a tuffaceous fluvial facies of the Jehol Group with its well-known Jehol Biota that includes the teleost *Lycoptera* and pelecypods, which were found in association with the holotypic skeleton (*16*). The matrix around the fossil is light green, massive, poorly sorted, tuffaceous, micaceous sandstone with fibrous gypsum. The light-colored, uncrushed bones were buried for the most part in articulation. The absence of laminated, fine-grained sediment or conchostracans characterizes the Lujiatun Beds of the Yixian Formation, dated to the late Early Cretaceous (Barremian-Aptian, ~125 Ma) (*16*). **Diagnosis**: Basal tyrannosauroid with a narrow accessory pneumatic fossa within the antorbital fossa dorsal to the maxillary fenestra, jugal suborbital ramus of particularly narrow depth (transverse width approximately 60% of vertical depth), and absence of a vertical crest on the iliac blade dorsal to the acetabulum.
16. See supporting material on *Science* Online.
17. E. J. Rayfield, *Zool. J. Linn. Soc.* **144**, 309 (2005).
18. E. Snively, D. M. Henderson, D. S. Phillips, *Acta Palaeontol. Pol.* **51**, 435 (2006).
19. J. H. Hurum, P. J. Currie, *Acta Palaeontol. Pol.* **48**, 161 (2003).
20. T. D. Carr, *J. Vert. Paleontol.* **19**, 497 (1999).
21. J. A. Hopson, in *Biology of the Reptilia*, C. Gans, Ed. (Academic Press, London, 1979), vol. 9, pp. 39–146.
22. J. W. Franzosa, thesis, University of Texas at Austin (2004).
23. D. K. Zelenitsky, F. Therrien, Y. Kobayashi, *Proc. R. Soc. London Ser. B* **276**, 667 (2009).
24. H. C. E. Larsson, P. C. Sereno, J. A. Wilson, *J. Vert. Paleontol.* **20**, 615 (2000).
25. F. Seebacher, *J. Vert. Paleontol.* **21**, 51 (2001).
26. F. Therrien, D. M. Henderson, *J. Vert. Paleontol.* **27**, 108 (2007).
27. K. M. Middleton, S. M. Gatesy, *Zool. J. Linn. Soc.* **128**, 149 (2000).
28. A. G. Smith, D. G. Smith, B. M. Funnell, *Atlas of Mesozoic and Cenozoic Coastlines* (Cambridge Univ. Press, Cambridge, 1994), pp. 1–38.
29. P. C. Sereno, S. McAllister, S. L. Brusatte, *PhyloInformatics* **8**, 1 (2005).
30. W. D. Matthew, B. Brown, *Am. Mus. Novit.* **89**, 1 (1923).
31. For final drafts of all figures, we thank C. Abraczinskas. For preparation of fossil material, we thank personnel of the Western Paleontological Laboratories and the Fossil Lab at the University of Chicago. For assistance with computed tomography imaging, we thank C. Straus and C. Wietholt; for preparation of paleohistologic sections, we thank E. Lamm and D. Varricchio. For examination of fossil material in their care, we thank X. Xu, M. Norell, and S. Hutt. Supported by the Whitten-Newman Foundation and the National Geographic Society (to P.C.S.). This is Publication 3 of the Chinese-American Dinosaur Expeditions.

Supporting Online Material

www.sciencemag.org/cgi/content/full/1177428/DC1
Materials and Methods
Figs. S1 to S8
Tables S1 and S2
References

8 June 2009; accepted 25 August 2009
Published online 17 September 2009;
10.1126/science.1177428
Include this information when citing this paper.

Deep-Sea Archaea Fix and Share Nitrogen in Methane-Consuming Microbial Consortia

Anne E. Dekas,* Rachel S. Poretsky, Victoria J. Orphan*

Nitrogen-fixing (diazotrophic) microorganisms regulate productivity in diverse ecosystems; however, the identities of diazotrophs are unknown in many oceanic environments. Using single-cell–resolution nanometer secondary ion mass spectrometry images of ^{15}N incorporation, we showed that deep-sea anaerobic methane-oxidizing archaea fix N_2, as well as structurally similar CN^-, and share the products with sulfate-reducing bacterial symbionts. These archaeal/bacterial consortia are already recognized as the major sink of methane in benthic ecosystems, and we now identify them as a source of bioavailable nitrogen as well. The archaea maintain their methane oxidation rates while fixing N_2 but reduce their growth, probably in compensation for the energetic burden of diazotrophy. This finding extends the demonstrated lower limits of respiratory energy capable of fueling N_2 fixation and reveals a link between the global carbon, nitrogen, and sulfur cycles.

Nitrogen-fixing (diazotrophic) bacteria and archaea convert dinitrogen (N_2) into ammonia (NH_3) for assimilation. Biological N_2 fixation counteracts the removal of bioavailable N by microbial processes such as denitrification and anaerobic ammonium oxidation (anammox) and provides a source of N to the majority of the biosphere that cannot directly assimilate N_2. Many photosynthetic cyanobacteria fix N_2 in ocean surface waters and have been the primary focus of studies on marine diazotrophy. Recently, a discrepancy between the calculated rates of oceanic denitrification and N_2 fixation has suggested that other less well–studied or currently unknown diazotrophic microorganisms may exist and fix substantial amounts of N_2 (*1*–*5*). Indeed, recent discoveries of new phylogenetically and physiologically diverse diazotrophs, including hyperthermophilic methanogens from hydrothermal vents (*6*), have shown that N_2 fixation can occur in extreme environments and localized habitats of enhanced productivity in the deep sea (*5*, *7*, *8*).

Here we show that syntrophic aggregates of archaea (of the ANME-2 group) and bacteria [*Desulfosarcina/Desulfococcus* (DSS)] mediating sulfate-dependent anaerobic oxidation of methane (CH_4) (AOM) in deep-sea sediments are capable of N_2 fixation. The ANME-2/DSS consortia have been studied in recent years both because of their potentially critical role in marine carbon cycling and their enigmatic obligate syntrophy (*9*, *10*). These consortia are most abundant in areas of high CH_4 concentration, such as cold seeps, but are present throughout continental margin sediments [(*9*) and references therein]. They currently represent the main filter for oceanic CH_4 release to the atmosphere, consuming up to 80% of naturally released CH_4 in marine sediments (*9*); however, the specific mechanism(s) coupling the ANME-2 and DSS cells remains unclear. Recent metagenomic sequencing of the ANME-2/DSS consortia identified the presence of nitrogenase genes required for N_2 fixation (*nif* genes) (*11*). This result, along with preliminary N isotope data, suggests that microbes within the consortia are able to fix N (*11*). We used submicron-scale ion imaging by nanometer secondary ion mass spectrometry (nanoSIMS) coupled to fluorescence in situ hybridization (FISH) to specifically identify the ANME-2 species as diazotrophs while detailing and quantifying patterns of N assimilation within the individual members of these metabolically interdependent consortia.

Sediment samples from an active CH_4 seep in the Eel River Basin, California, USA, were collected and anaerobically incubated with CH_4 and one of several ^{15}N-labeled N sources (*12*) (table S1). Nitrogen fixation, as demonstrated by the assimilation of ^{15}N from $^{15}N_2$ in coaggregated ANME-2 and DSS cells, occurred in all AOM consortia measured after 6 months of incubation with CH_4 (*12*) (Fig. 1, A and B, and Fig. 2A). ^{15}N enrichment within the consortia was as high as 10.5 ^{15}N atom %, which is 26 times the highest value observed in unlabeled ANME-2/DSS

Division of Geological and Planetary Sciences, California Institute of Technology, Pasadena, CA 91125, USA.

*To whom correspondence should be addressed. E-mail: vorphan@gps.caltech.edu (V.J.O.); dekas@gps.caltech.edu (A.E.D.)